




# Development of a musculoskeletal shoulder model considering anatomic joint structures and soft-tissue deformation for dynamic simulation

Taku Tazawa<sup>1,4</sup> · Masaya Yasui<sup>2</sup> · Shun Otsuka<sup>3</sup> · Naoyuki Hatayama<sup>3</sup> · Munekazu Naito<sup>3</sup> · Shigemichi Ohshima<sup>1</sup> · Hiroki Yokota<sup>1</sup> 

Received: 27 November 2023 / Accepted: 15 April 2024 / Published online: 2 May 2024  
© The Author(s), under exclusive licence to Japanese Association of Anatomists 2024

## Abstract

The shoulder joint has a high degree of freedom and an extremely complex and unstable kinematic mechanism. Coordinated contraction of the rotator cuff muscles that stop around the humeral head and the deltoid muscles and the extensibility of soft tissues, such as the joint capsule, labrum, and ligaments, contribute to shoulder-joint stability. Understanding the mechanics of shoulder-joint movement, including soft-tissue characteristics, is important for disease prevention and the development of a device for disease treatment. This study aimed to create a musculoskeletal shoulder model to represent the realistic behavior of joint movement and soft-tissue deformation as a dynamic simulation using a rigid-body model for bones and a soft-body model for soft tissues via a spring–damper–mass system. To reproduce the muscle-contraction properties of organisms, we used a muscle-expansion representation and Hill’s mechanical muscle model. Shoulder motion, including the movement of the center of rotation in joints, was reproduced, and the strain in the joint capsule during dynamic shoulder movement was quantified. Furthermore, we investigated narrowing of the acromiohumeral distance in several situations to induce tissue damage due to rotator cuff impingement at the anterior–subacromial border during shoulder abduction. Given that the model can analyze exercises under disease conditions, such as muscle and tendon injuries and impingement syndrome, the proposed model is expected to help elucidate disease mechanisms and develop treatment guidelines.

**Keywords** Shoulder joint · Muscle tonus · Periarthritis

## Introduction

Among the locomotors of the human body, the shoulder joint, in particular, has a high degree of freedom (DOF) and an extremely complex and unstable kinematic mechanism (Veeger & van der Helm 2007). Muscle tension in the rotator

cuff muscles that stop around the humeral head and deltoid muscles and the extensibility of soft tissues, such as the joint capsule, labrum, and ligaments, contribute to shoulder-joint stability. For example, the rotator cuff consists of four muscles—namely, the subscapularis, supraspinatus, infraspinatus, and teres minor—and is responsible for stabilizing the bony head by pulling the entire joint capsule toward the scapula (Escamilla, 2009; Neumann 2016). The joint capsule and surrounding soft tissues provide mechanical support to the glenohumeral joint via passive tension during shoulder motion, inhibiting excessive rotational translation movements (Neumann 2016; Lugo et al. 2008). Understanding these mechanics is particularly important in the medical and welfare fields because it can lead to the prevention of diseases, such as periarthritis, and the development of devices for treating shoulder diseases.

Recently, several studies on the computational simulation of shoulder movement have been published. In some studies, bones and muscles were regarded as elastic bodies

✉ Hiroki Yokota  
yokota@meijo-u.ac.jp

<sup>1</sup> Department of Mechanical Engineering, Meijo University, 1-501 Shiogamaguchi, Tempaku-Ku, Nagoya-Shi, Aichi, Japan

<sup>2</sup> Department of Judo Seifuku and Health Sciences, Tokoha University, 1230 Miyakodacho, Kita-ku, Hamamatsu-shi, Shizuoka, Japan

<sup>3</sup> Department of Anatomy, Aichi Medical University, 1–1 Yazakokarimata, Nagakute-shi, Aichi, Japan

<sup>4</sup> Present Address: ASAHI INTECC CO., LTD., Aichi, Japan

that deform, and numerical analysis was performed using the finite element method based on the use of boundary integral operators for constructing the element stiffness matrices for an elastic spring (Islan et al. 2018; Péan et al. 2019; Zheng et al. 2017). Conversely, simulation studies without the finite element method have reported that the bones and muscles of the human shoulder are regarded as a rigid body and a set of lines in multibody simulation performed using equations of motion (Aurbach et al. 2020; Flores-Hernandez et al. 2019; Chadwick et al. 2014; Leschinger et al. 2019). Although finite element simulations of the human body can account for biomaterial deformation, they are computationally expensive and make dynamic motion analysis, such as large swinging movements with arms, difficult. In contrast, dynamic simulation using a rigid body and muscle modeled as a set line, which is better suited for dynamic analysis with a reduction in computational efficiency, can perform dynamic motion analysis for sports and other activities; however, accounting for soft-tissue deformation, such as muscle expansion, due to muscle contraction and contact between surrounding tissues is difficult using this method. Furthermore, in motion analysis, the glenohumeral joint of the shoulder is often subject to constraints, such as a 3-DOF ball-socket joint. Realistic joint movements, such as the movement of the center of rotation during large motions, are difficult to evaluate, regardless of the surrounding soft tissues, such as the joint capsule and labrum.

Therefore, this study aimed to create a musculoskeletal shoulder simulation model that can represent the behavior of soft tissues while allowing forward dynamic operations using a rigid-body model for bones and a soft-body model for soft tissues, such as muscles and the joint capsule, via a spring–damper–mass system, which replaced the straight-line muscle model and ball-and-socket joints based on dynamic operations. The spring–damper–mass system is one type of a mechanical model that utilizes a sequential method to solve the equations of motion for mass particles considering the restoring force and damping force. We believe that this system shares similar characteristics with soft tissues in living organisms and tends to return to its original shape even when deformed by external forces, such as stretching, while damping during the process; therefore, we applied it to the above soft-body model. By incorporating cadaver findings and kinematic parameters into the rigid/soft-body model, we constructed a realistic shoulder-joint simulation model. In this simulation, muscle contraction based on Hill's model was reproduced, and the displacement of the center of joint rotation and the strain distribution in the joint capsule were visualized. Furthermore, we analyzed under the assumption of actual impingement syndrome by measuring the acromiohumeral distance (AHD) in the proposed system.

## Materials and methods

### Cadaver specimens

The examined cadaver was of an 88-year-old woman with no signs of trauma or surgical scars. Experimental measurements using the cadaver were performed in compliance with a protocol reviewed by the ethical committee of the Aichi Medical University (Permit Number: 2019-M003). Furthermore, written informed consent for scientific investigations in general was obtained from all body donors prior to death. The cadaver was fixed with embalming fluid containing 7% formaldehyde, 6% glycerol, and 38% alcohol.

### Shoulder-joint dynamic model

Figure 1a–d shows the shoulder-joint model developed in this study. In the dynamic simulation system, the model consists of three bones with rigid bodies, two joint capsules, four ligaments, one labrum, and five muscles with soft bodies. Bone models were created from cadaver bones (Fig. 2a) and converted to 3D polygons (Fig. 2b) using a Digital Imaging and Communications in Medicine computed tomography (CT) data set. The constructed 3D polygons have complex vertex arrangements, and it is difficult to simulate contact processes on a computer because of unstable calculations. Therefore, the convex hull and volumetric hierarchical approximate convex decomposition algorithm (Mamou et al. 2016; Müller et al. 2013) were applied to perform contact processing. The smallest polygon that contains all the given points was called a convex hull. Using a convex hull for a rigid-body model speeds up and stabilizes the computation of the contact process during simulation (Mamou et al. 2016; Müller et al. 2013). However, applying convex hulls to the entire object, such as the entire scapula, results in a simple shape that cannot mimic the bone morphology. Therefore, we have divided each bone (e.g., the scapula) and applied convex hulls to each part automatically by use of Blender, an open-source 3D computer graphics software toolset, which enabled calculations while maintaining the original bone shapes, as shown in Fig. 2c, and achieve contact processing using convex hulls. Regarding the arrangement of each bone, we located the position where each articular surface connects by referring to the anatomic literature (Neumann 2016) as follows: the orientation of the clavicle deviated 20° posterior to the frontal plane, and the orientation of the scapula deviated 35° anterior to the frontal plane. The humeral head was rotated posteriorly approximately 30° within the horizontal plane. BulletPhysics (Bullet 2015), a dynamics analysis library, was used to load the created 3D polygons into the computer system, and the humerus, scapula, and

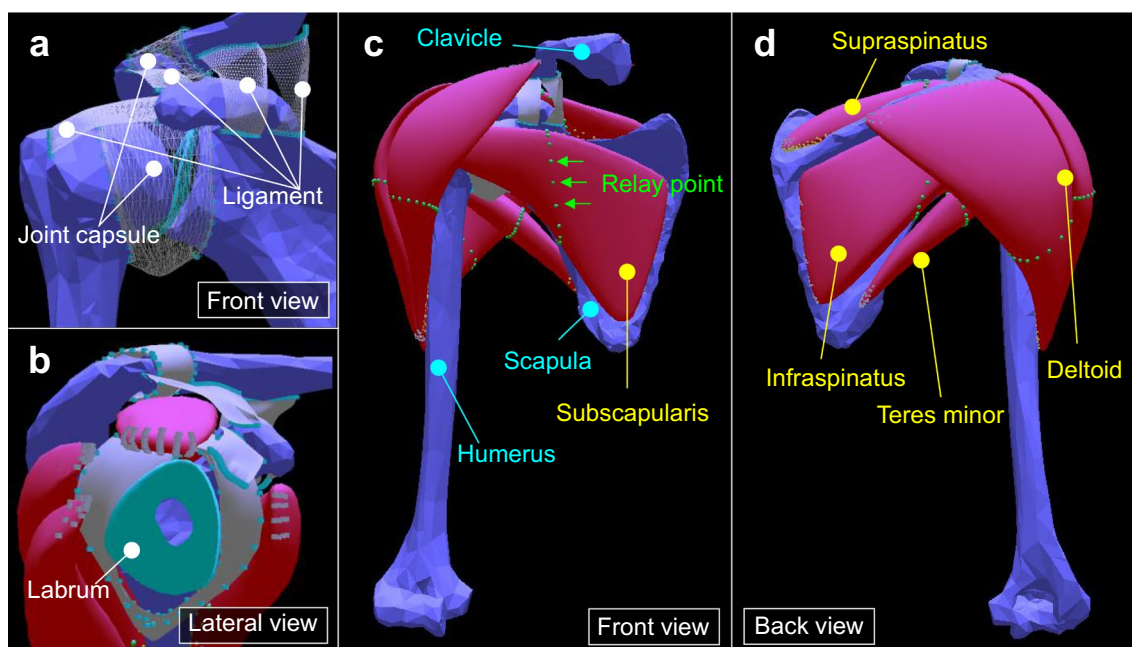
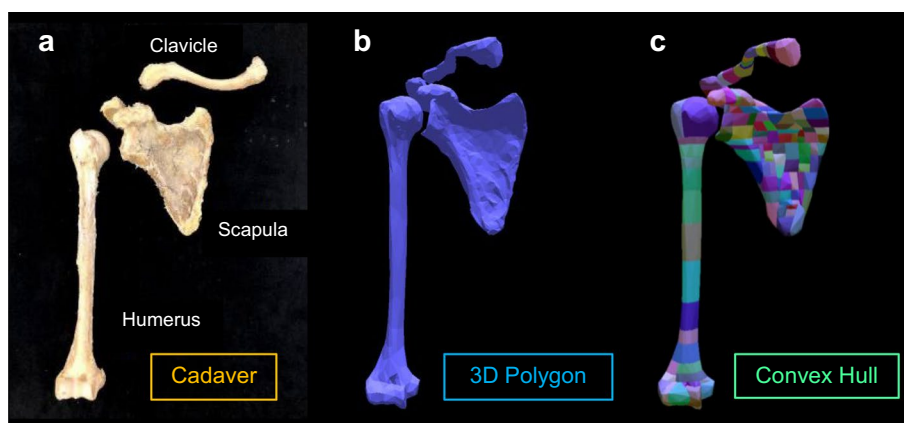


**Fig. 1** Overview of the constructed shoulder-joint model for dynamic simulation. Here, **a** shows a wire frame view of the joint capsule and ligament models, and **b** shows a view of the glenoid fossa from the side of the humeral head. Furthermore, **c** shows a view of the entirety of the constructed model from the front side, and **d** shows a view of

the entirety of the model from the back. Bones are represented by a rigid-body model, whereas muscles and soft tissues are represented by a soft-body model. The green node represents the relay point of the muscular contraction force

**Fig. 2** The procedure for creating a convex full model of the shoulder bones for numerical simulation. Here, **a** shows a bone extracted from a cadaver, **b** shows a 3D polygon constructed from a CT image of the cadaver, and **c** shows a 3D polygon that has been decomposed into multiple convex hulls and combined



clavicle were placed as rigid-body models. A cadaver was used to determine the mass of the sampled bones. Based on the measured values, the mass parameters of the rigid-body model were determined.

The joint capsule, labrum, coracohumeral ligament, acromioclavicular ligament, and coracoclavicular ligament were used as the soft-tissue models (Fig. 1). A spring–damper–mass system (Fig. 3a) was used to construct soft tissues as soft-body objects, which were used to realize shoulder-joint motion by stretching and contracting in response to external forces transmitted from the bones. The muscles were modeled as the rotator cuff (i.e., subscapularis,

infraspinatus, supraspinatus, and teres minor) and deltoid muscles (Fig. 1) and were constructed as soft objects and soft tissues connected to the bone. The origin and insertion of each muscle were determined based on the shape of the constructed bone and the cadaver findings. The muscle model was created from computational surface meshes that represent the muscle path based on the BodyParts3D dataset (Parts3D/Anatomography, 2008), considering the cadaveric shape. Furthermore, when a muscle-contraction force was applied, the model expanded in the direction normal to the mesh surface, reproducing the change in muscle path caused by muscle expansion (Fig. 3b).

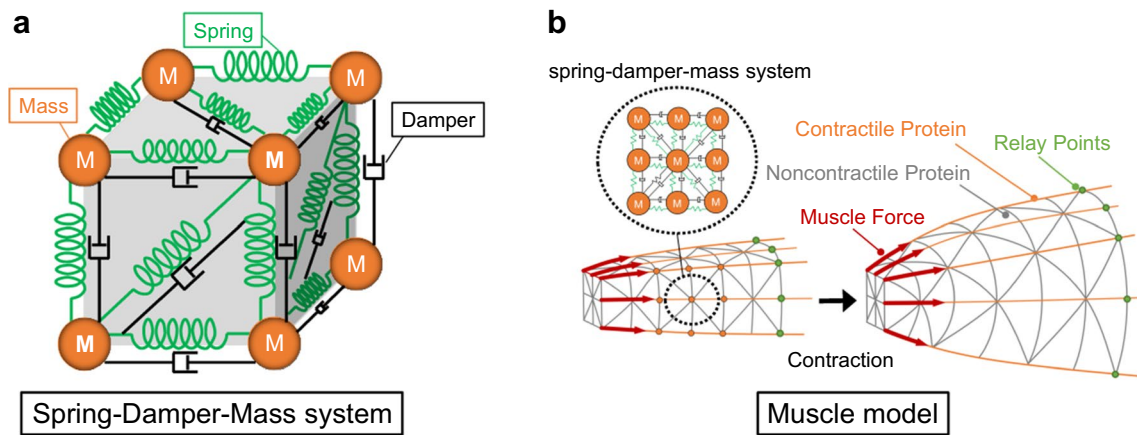


**Fig. 3** The figure illustrates how the muscle paths change due to expansion as the muscle contracts. For all vertices, the muscle model is represented by a spring–damper–mass system. The orange line represents a contractile protein, whereas the gray line represents a non-

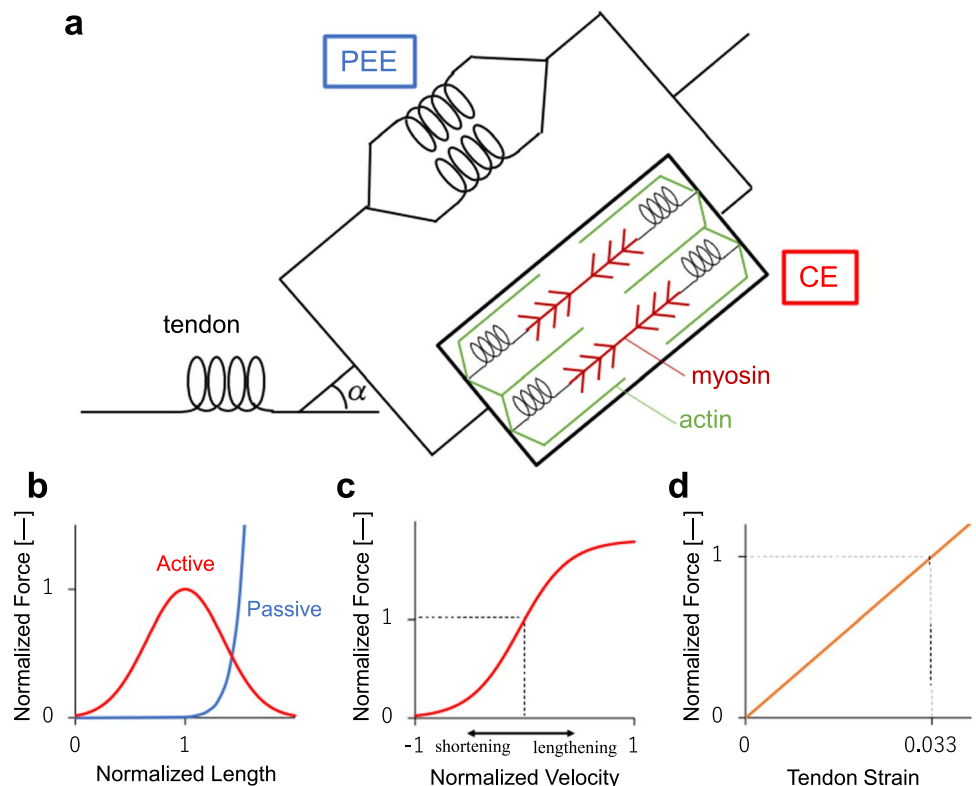
contractile protein. The green dots represent the relay points of the contractile force. The red arrows indicate the direction of the muscle tension. Muscle tension is applied to the relay point from the origin and insertion

**Hill model reproduction of muscle contraction properties**

To reproduce the muscle-contraction properties of an organism, Hill’s mechanical model was used (Hill 1938; Zajac 1989). As shown in Fig. 4a, the model comprised three parts, namely, contractile element (CE), parallel

elastic element (PEE), and tendon. This numerical model had nonlinear output properties that varied with muscle length and contraction velocity, and linear output properties regarding tendon strain (Fig. 4b–d). The numerical parameters used for these model parts were determined based on previous literature (Thelen 2003; Buchanan et al. 2004; Gordon et al. 1966). The angle of the muscle fiber relative to the tendon (pennation angle) was also considered.

**Fig. 4** The numerical muscle model **a** shows the schematic diagram of the Hill’s model. CE is the contractile element, PEE is the parallel elastic element, and  $\alpha$  is the pennation angle. Moreover, **b** shows the length–tension relationship of CE and tendon, with Active and Passive representing the CE and tendon properties, respectively, **c** shows the velocity–tension relationship for CE, and **d** shows the elongation–tension relationship of tendon. The complex physiological and mechanical interactions that occur between actin and myosin cause CE to contract





### 1) CE

When the muscle-fiber length is close to its optimal length, CEs comprising contractile proteins exhibit greater contractility. Based on previous literature, this property is expressed using the following Gaussian function, where  $b$ ,  $c$ , and  $d$  are parameters that determine the shape of the Gaussian function and are set to 1, 1, and 0.35, respectively (Thelen 2003; Buchanan et al. 2004; Gordon et al. 1966). Moreover,  $l$  is the normalized muscle-fiber length.

$$F_{\text{act}}^l = \text{bexp}\left(-\frac{(1-c)^2}{2d^2}\right) \quad (1)$$

### 2) PEE

When the muscle-fiber length exceeds the optimal length, PEEs comprising noncontractile proteins exert force. This property is expressed by the following exponential function:

$$F_{\text{pas}} = \frac{e^{10(l-1)}}{e^5} \quad (2)$$

### 3) Muscle force and contraction speed

The tension exerted by the CE varies with the rate of contraction and is expressed by the following sigmoidal function, where  $\beta$  and  $\gamma$  are parameters that determine the shape of the sigmoid function and are set to 4.46 and  $-0.05$ , respectively. Moreover,  $\gamma$  is the normalized contraction velocity of the muscle.

$$F_{\text{act}}^v = \frac{1.8}{1 + e^{-\beta(v-\gamma)}} \quad (3)$$

### 4) Tendon

Tendons are stretched passively by muscle contraction, and the force exerted varies with the rate of stretch,  $\epsilon_t$ . It is expressed by the function proportional to  $\epsilon_t$ , as follows:

$$F^t = 33\epsilon_t \quad (4)$$

Pennation angle is defined as the angle between the direction of the muscle fibers and the tendon axis (i.e., the line of action), and the actual tension applied to the bone in the direction of the line of action is the cosine component with respect to the tension exerted by the muscle fibers.

Considering the aforementioned characteristics, the total tension of the muscle is expressed using the following equation:

$$F = (a \cdot F_{\text{max}} \cdot F_{\text{act}}^l \cdot F_{\text{act}}^v + F_{\text{max}} \cdot F_{\text{pas}}) \cos \alpha = F^t \quad (5)$$

Here,  $a$  is the muscle activity,  $F_{\text{max}}$  is the maximum muscle tension, and  $\alpha$  is the pennation angle. The maximum tensile force has been reported to be proportional to the physiological cross-sectional area (PCSA), and this study calculated the maximum tensile force from the PCSA (Enoka 2015; Neumann & Garceau 2015). The mass, PCSA, and pennation angle were measured using a cadaver (Fig. 5a and b). Table 1 shows the mass, PCSA, and pennation angle determined from the measurement results and previous literature (Holzbaur et al. 2005).

### Constructed simulation system

The simulation system has a GUI environment using OpenGL, which allows for individual manipulation of muscle activity and real-time modification of physical parameters. This system with various changeable parameters analyzes diseases based on different shoulder-joint movements. Furthermore, expressing functional hypertonia/weakness is

**Fig. 5** The cadaveric study for measuring muscle parameters using numerical simulation. Here, **a** shows an overall view of the cadaveric shoulder from the front side, and **b** shows an overall view of the cadaveric shoulder from the back side. The pennation angles of the shoulder muscles (i.e., subscapularis, infraspinatus, supraspinatus, teres minor, and deltoid muscle) were measured on the cadaver

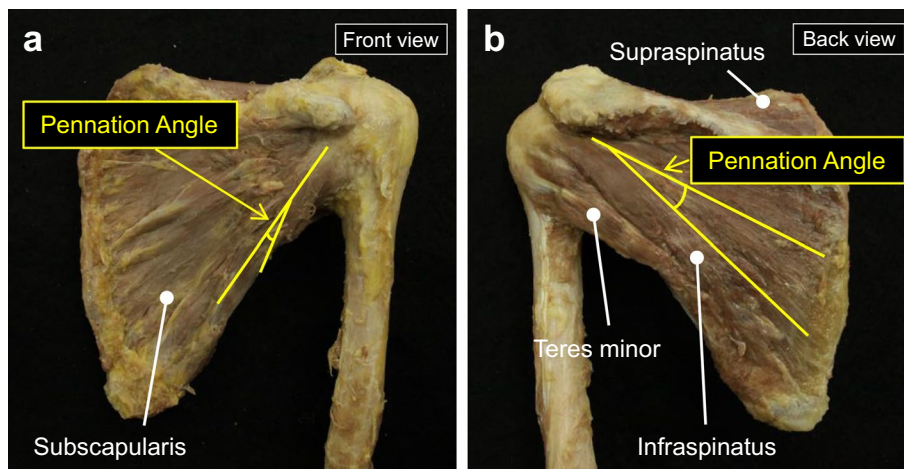


**Table 1** Determined mass, PCSA, and pennation angle parameters

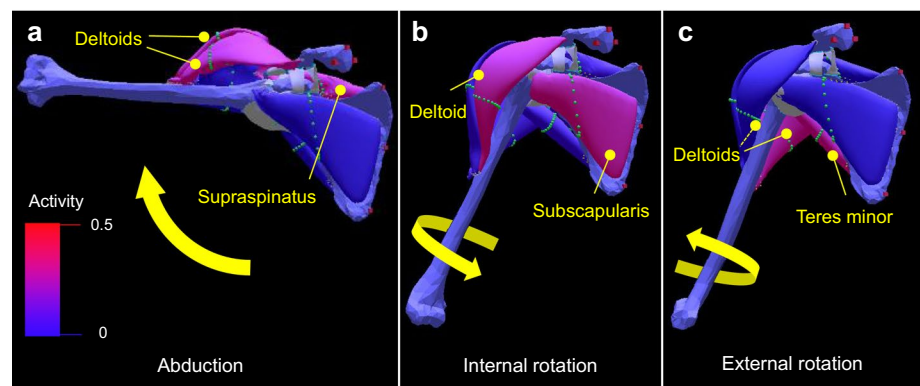
Muscle	Mass (g)	PCSA (cm <sup>2</sup> )	Pennation angle (°)
Subscapularis	53	15.53	14
Infraspinatus	41	10.71	20
Supraspinatus	25	5.99	7
Teres minor	14	3.18	10
Deltoid anterior	20	4.11	–
Deltoid middle	55	16.5	10
Deltoid posterior	22	4.40	–

possible by increasing/reducing muscle activity in individual muscles and considering interactions between biologic tissues. Furthermore, bones, muscles, and soft tissues can be visually shown or hidden, and wires can be shown to visualize the behavior of the joint capsule, labrum, and other tissues not visible from the outside.

### Creation of shoulder-joint movement

To evaluate shoulder-joint movement using the constructed model, muscle tension calculated using Hill's model was added to the origin and insertion of the humerus, scapula, and clavicle. By searching and setting the activation level of the muscle groups responsible for abduction, internal rotation, and external rotation, we reproduced these movements when each muscle group worked predominantly. Furthermore, the simulation reproduced the physiologic muscle tonus of the rotator cuff by applying weak muscle tension as a sustained force. Physiologic muscle tonus is a state of sustained weak muscle contraction through the sequential flow of nerve impulses that help maintain normal body posture (Styer-Acevedo 1999; Masi & Hannon, 2008). Analyzing this constant muscle tone is important to assess shoulder movement disorders caused by abnormal muscle tonus.

**Fig. 6** Simulation results are shown when **a** the supraspinatus and anterior and middle deltoid fibers; **b** the subscapularis and anterior deltoid fibers; and **c** the infraspinatus, teres minor, and posterior deltoid fibers are predominantly activated



### Visualization of strain distribution in the joint capsule

The amount of strain in the joint capsule during shoulder-joint motion was quantified by visualizing the distribution using the difference values of the vertex coordinates of the joint capsule polygon and quantifying the amount of mechanical loading. The difference values were defined from the initial position of the joint capsule, as shown by Fig. 1. The joint capsule was divided into six sections (i.e., anterior upper, middle, and lower and posterior upper, middle, and lower sections), and the amount of strain was measured at each abduction angle.

### Analysis of subacromial impingement syndrome

To evaluate the relationship between muscle activations and AHD narrowing during abduction for discussing the possibility of causing subacromial impingement syndrome, we assumed the following three shoulder situations: “no abnormal findings,” “weakness of the rotator cuff,” and “precedence of the deltoid.” In “no abnormal findings,” we set a gradual increase in the activation level of all muscles to reproduce abduction. In “weakness of the rotator cuff,” we set a weak-activation level of the rotator cuff muscles to assume a state of functional weakness. In “precedence of the deltoid,” we assumed the excess action of the deltoid muscle by the collapse of the force couple of the shoulder muscles.

## Results

### Reproduction of shoulder-joint motion

The relationship between activity levels of each muscle and shoulder motion behavior was revealed. Figure 6 shows the simulation results with each muscle activated as mentioned in Sect. “Constructed simulation system”. The dominant and nondominant muscle activation levels were 0.4 and

0.05, respectively, in this simulation. In Fig. 6a, when the supraspinatus muscle and anterior and middle deltoid fibers acted predominantly, abduction was activated. In Fig. 6b, when the subscapularis and anterior deltoid fibers acted predominantly, internal rotation was activated. In Fig. 6c, when the infraspinatus, teres minor, and posterior deltoid muscles acted predominantly, external rotation was activated. In Fig. 6b and c, the slight abduction was also activated by anterior/posterior deltoid muscle.

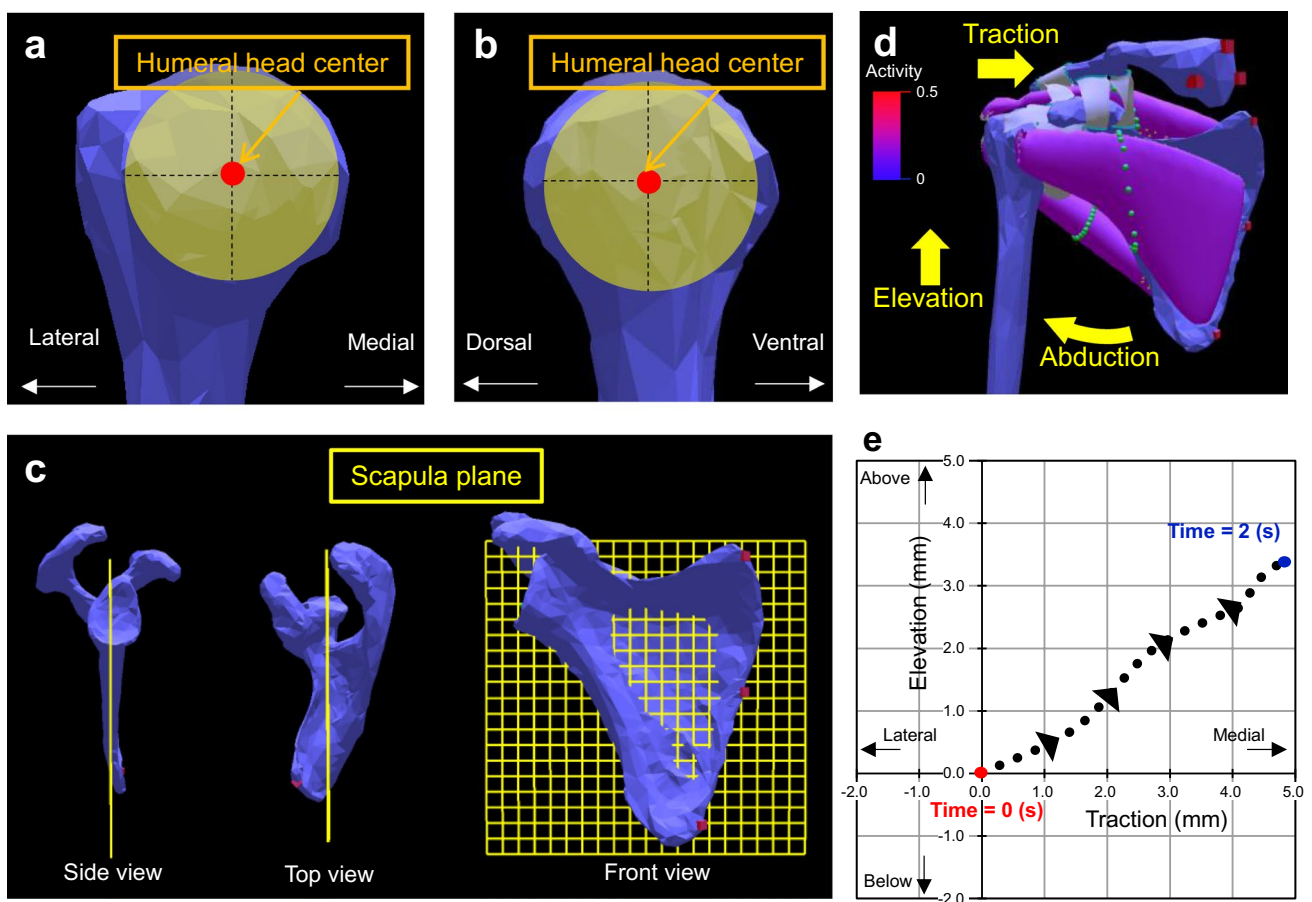
Figures 7a–c show the humeral head center and scapular plane. During the simulation of physiological muscle tonus, the trajectory of the humeral head center in the scapular plane was measured. The activation levels of the rotator cuff were 0.2 in this simulation. Figures 7d and e show the results of the simulation and measurement, respectively. In the simulation, the rotator cuff pulled, elevated, and abducted the head of the humerus and subsequently maintained this steady posture, as shown in Fig. 7d. As the muscle contracted, the center of the humeral head was elevated and attracted to the glenoid, as shown in Fig. 7e. In this

simulation, approximately 3.5-mm elevation and 4.5-mm attraction to the glenoid fossa were observed.

### Strain distribution in the joint capsule during shoulder abduction

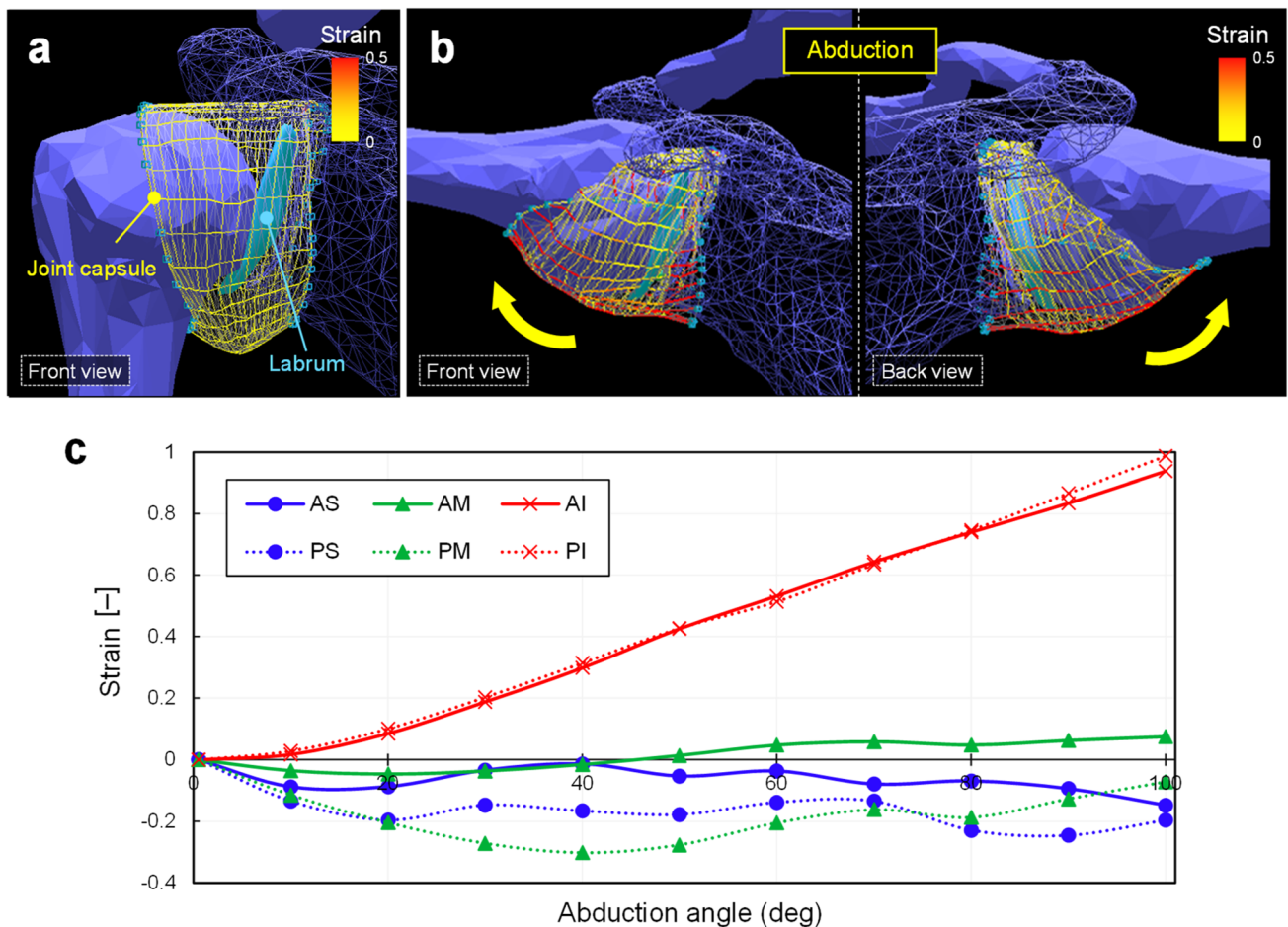
The relationship between shoulder abduction behavior and strain distribution in the joint capsule was revealed. Figure 8a and b show the visualization results of the strain distribution that occurred during the replicated abduction movement described in Sect. "Reproduction of shoulder-joint motion". When the amount of strain from the initial condition approached 0, the mesh was displayed in yellow, and when it approached 0.5, the mesh turned red. The humeral head and joint capsule were extended with contact, as shown in Fig. 8b. Deformity due to contact of the labrum with the humeral head can also be observed.

Figure 8c shows a graph of the relationship between the abduction angle and the amount of strain. As the abduction angle increased, the inferior portion of the joint capsule



**Fig. 7** Movement of humeral head center in the scapular plane. Here, **a** shows a view of the humeral head from front side; **b** shows a view of the humeral head from the glenoid fossa side. The bone head is replaced by a sphere to define the center of the bone head; **c** shows

the determined scapula plane; **d** shows the results of simulating physiological muscle tonus; and **e** shows the trajectory of the epiphysis center in the scapular plane during simulation at physiological muscle tonus



**Fig. 8** Visualization and measurement results of the joint capsule strain. **a** Initial position of the joint capsule. **b** The strain distribution of the joint capsule in the abduction. The joint capsule is shown as a wire, and the deformation of the labrum within the capsule is also visible. **c** Relationship between the joint capsule strain and abduction

lengthened, whereas the superior portion of the joint capsule was lax. After 50° of abduction, the anterior middle joint capsule lengthened. The posterior middle joint capsule exhibited no such tendency but relaxed with the angle of abduction.

### AHD in abduction

Figures 9a–c depicts the time history of muscle activation in the three situations. In Fig. 9a, “no abnormal findings” showed a gradual increase in the activation level of all muscles, indicating that the deltoid and rotator cuff muscles cooperate during abduction due to the predominance of the anterior and middle deltoid fibers and the supraspinatus, which are the main action muscles during abduction. In Fig. 9b, “weakness of the rotator cuff” condition indicates that the rotator cuff muscles are in a

state of functional weakness by reducing the activity of these muscles compared with that of muscles under the “no abnormal findings” condition. In Fig. 9c, “precedence of the deltoid” condition describes the excess action of the deltoid muscle by increasing the total deltoid muscle activity earlier than that under the “no abnormal findings” condition. In Fig. 9d, AHD was defined as the distance between the attachment of the supraspinatus muscle to the greater tubercle and acromion. The relationship between the AHD and abduction angle measured during simulation is shown in Fig. 9e. Figure 9e also shows that under the “weakness of the rotator cuff” and “precedence of the deltoid” conditions, the AHD significantly decreased by approximately 20°–50° of the abduction angle compared with that under the “no abnormal findings” condition. Almost no difference in the AHD was observed between abduction angles of 0°–20° and 50°–110°.



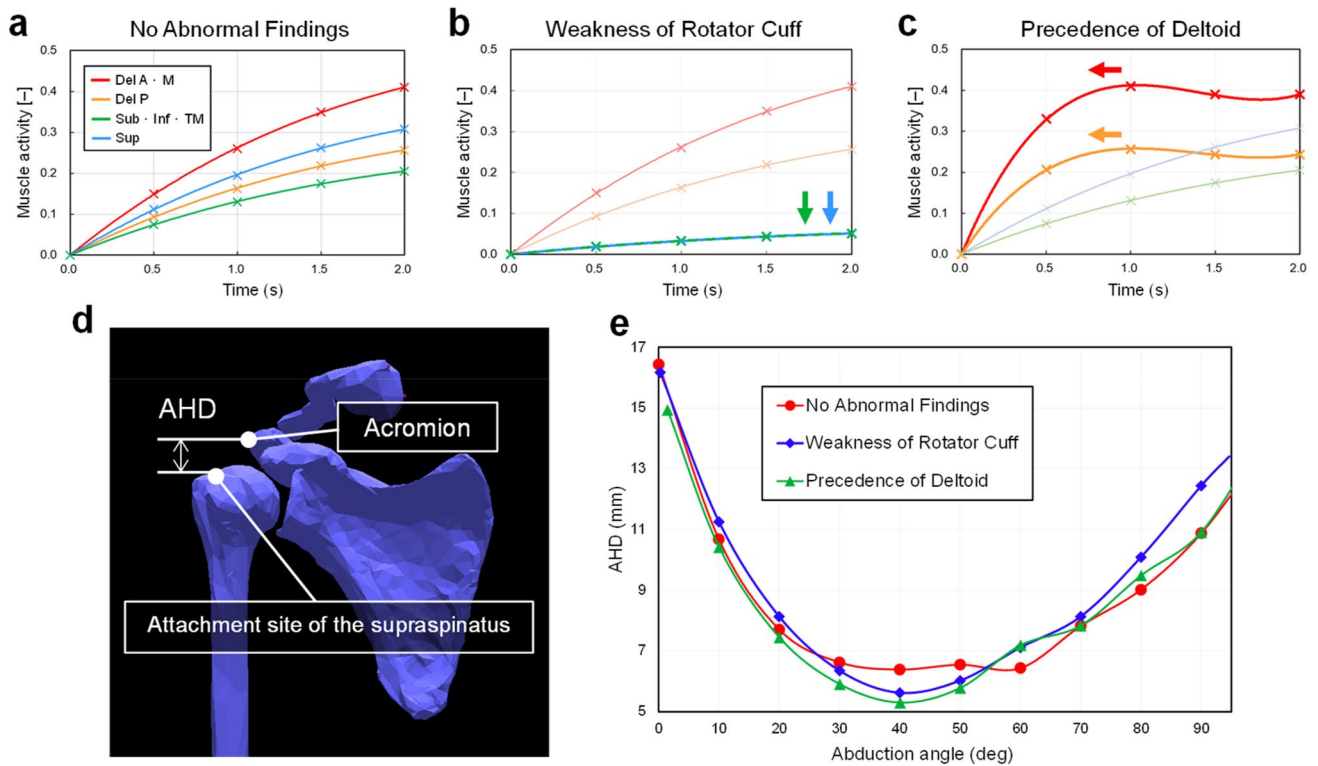


**Fig. 9** Measurement of AHD in three shoulder situations in the simulation. Here, **a** shows a graph of the time variation of muscle activation during the “no abnormal findings” simulations; **b** illustrates a graph of time variation of muscle activation during the “weakness of the rotator cuff” simulations; **c** depicts the time variation graph of muscle activation during the “precedence of the deltoid” simulations.

Cubic spline curves, with markers indicating control points, represent changes in muscle activation. **d** shows the location of AHD measurement. The distance between the attachment of the greater tubercle of the supraspinatus and the inferior edge of the acromion was measured. **e** shows the relationship between the AHD and abduction angle under each condition graphically

**Discussion**

This study used dynamic musculoskeletal modeling of the shoulder-joint with bones, muscles, and soft tissues. Hill’s model was implemented for the muscles. Forward dynamic simulation was analyzed, which included the reproduction of shoulder-joint motion, measurement of the joint capsule extension rate, and measurement of the AHD during abduction.

In Sect. “[Reproduction of shoulder-joint motion](#)”, we simulated the predominant activation of the muscles responsible for abduction, internal rotation, and external rotation and the physiologic muscle tonus of the rotator cuff to reproduce shoulder-joint motion, including the movement of the center of rotation, during abduction. These results were consistent with the actions of the rotator cuff and deltoid in previous literature (Escamilla, 2009; Neumann 2016), indicating that the shoulder model was similar to the actual shoulder joint. This study focused on the glenohumeral and acromioclavicular joints and constructed models for these joints. The actual shoulder joint comprises four joints: the sternoclavicular joint, acromioclavicular joint, scapulothoracic joint, and

glenohumeral joint. To account for the combined motion of these joints, such as the scapulohumeral rhythm, soft tissues other than those discussed in this article must be modeled.

When physiological muscle tonus was simulated, the rotator cuff was found to elevate the humeral head and attract it to the glenoid fossa. These results suggest that excessive tonus of the rotator cuff causes abnormal upward translation of the humeral head, leading to inflammation of the supraspinatus and other muscles in the subacromial space due to the interacting force. Conversely, decreased-rotator cuff tonus may reduce traction on the glenoid fossa, resulting in glenohumeral instability. Studies have reported that causing a force imbalance among rotator cuff muscles may impact functional task performance, altering glenohumeral joint contact forces, potentially contributing to instability or joint damage risk (Vidt et al. 2018; Marchi et al. 2014). In future studies, it is expected that the use of simulation analysis with variable parameters such as activation levels in combination with quantitative analysis such an electromyogram will help to elucidate the physiologic mechanism of muscle tonus.

First half of Sect. "Strain distribution in the joint capsule during shoulder abduction" depicts the distribution of strain in the shoulder-joint capsule in response to abduct the shoulder joint. In the latter half of Sect. "Strain distribution in the joint capsule during shoulder abduction", amount of strain of joint capsule with respect to angle change of shoulder joint was quantified. The inferior joint capsule stretched with the abduction angle and acted as a stabilizer during abduction by increasing the tension. Studies have reported that the middle glenohumeral ligament, located in the anterior middle of the joint capsule, is elongated at 45°–90° of abduction (Debski et al. 1999; Massimini et al. 2012; Yang et al. 2010) and that the axillary recess and inferior glenohumeral ligament are tensed during abduction (Massimini et al. 2012; Warner et al. 1992), which is consistent with our findings. The glenohumeral ligament, located in the anterior superior portion of the joint capsule, relaxes primarily at external rotation  $\geq 35^\circ$ –45° (Massimini et al. 2012; Yang et al. 2010); however, in this study, relaxation was observed at external rotation of  $\geq 0^\circ$ . This difference could be due to the initial elongation of the joint capsule. It has also been reported that contracture of the posterior joint capsule causes limited range of motion of the glenohumeral joint (Moskal et al. 1999). Future developments will examine the amount of joint capsule strain during shoulder-joint movement to determine effective stretching positions for joint contractures.

In Sect. "AHD in abduction", we investigated how changing muscle activation during abduction affected the AHD. In subacromial impingement syndrome, the humeral head deviates upward, resulting in a narrowing of the AHD, which causes tissue damage due to rotator cuff impingement at the anterior–subacromial border during shoulder motion (Harrison & Flatow 2011; Garving et al. 2017). Furthermore, investigating the factors that influence the width of the subacromial space during abduction is critical (Kibler et al. 2013; Akkaya et al. 2017). Herein, we hypothesized that the action of the rotator cuff and deltoid muscles in attracting the humeral head to the glenoid fossa and elevating the humerus is related to AHD narrowing; therefore, we investigated their relationship. Results demonstrated that the collapse of the force couple due to functional weakness of the rotator cuff and overactivity of the deltoid muscles caused AHD narrowing. Studies have shown that the rotator cuff muscles can exert a downward force on the humeral head during abduction (Halder et al. 2001; McCully et al. 2007) and are necessary to neutralize the upward translational effect of the humeral head from the strong deltoid contraction, particularly during the initial movement of abduction (Chopp & Dickerson 2012; Paletta et al. 1997; Sharkey & Marder 1995). The same can be said for the results of this study. Furthermore, studies have reported that the shortest AHD varies with abduction angle, with the shortest AHD occurring between the attachment of the greater tubercle of

the supraspinatus muscle and the acromion in the 35°–70° abduction range (Giphart et al. 2012). In this study, the AHD decreased from 20° to 60°, which is reasonable considering the scapulohumeral rhythm. In this study, the AHD was defined as the area between the attachment of the supraspinatus muscle to the greater tubercle and the acromion. According to previous studies, the shortest AHD is between the acromion and the articular surface of the humeral head at 20°–35°, between the attachment of the supraspinatus to the greater tubercle and the acromion at 35°–70°, and between the acromion and the proximal humerus at 70° or greater (Giphart et al. 2012). By redefining the AHD using the aforementioned points, analyzing the impingement syndrome in more detail will be possible, which will aid in the development of appropriate treatment methods.

This study has some limitations. First, the material parameters of the soft-body objects, such as the muscle-contraction parameters described in Sect. "Shoulder-joint dynamic model", were set to appropriate values based on previous studies. A future challenge will be to apply the simulation parameters of real muscles and soft tissues using surface electromyogram to the individual patient model and develop a system for tailor-made medicine. Second, the muscle activation level of each muscle, which is a changeable parameter in real-time simulation, was determined to reproduce realistic shoulder movement in this study. Verifying the validity of these values is difficult because the electrical activity of the rotator muscles is immeasurable using surface electromyogram. Therefore, estimating the activation value of inner muscles using the inverse dynamic simulation method with a musculoskeletal model in future work is necessary. Third, this study presented a method for creating a shoulder model that can be tailored for an individual. In the creating process, a cadaver's bone geometry was used as the basis for the model, which may have contained individual bias in the shoulder-joint motion. In future, it will be necessary to construct models from multiple participants using CT scanning and conduct motion analysis to further verify the validity of the models.

We developed a dynamic musculoskeletal simulation model of the shoulder joint and surrounding tissues, considering the anatomic joint structure and soft-tissue deformation. Several muscle contractions were activated to simulate shoulder abduction, internal rotation, and external rotation. The amount of strain in the joint capsule was quantified and visualized using colors to represent changes in the distance between the vertex coordinates in the joint capsule model during movement. The effect of force couple collapse on the AHD was investigated by measuring the AHD during abduction simulation. These results suggest that this simulation system can contribute to the understanding of the underlying mechanisms of various disorders, such as muscle damage and impingement syndrome, and the treatment

of these disorders. In future, as the number of muscle and soft-tissue models in this simulation system grows, it will be able to reproduce the scapulohumeral rhythm and complex shoulder-joint motions to reveal the details of inertial dynamic dislocation disorders and apply simulation parameters for individual physical properties of body tissues for tailor-made medicine.

**Acknowledgements** The authors sincerely thank those who donated their bodies to science so that anatomic research could be conducted. Results from such research can increase humankind's overall knowledge, which can subsequently improve patient care. Therefore, these donors and their families deserve our highest gratitude. The authors thank Kazuto Arimura, Yoshiko Kunita, and Yohei Maruyama for their assistance.

**Authors' contributions** TT and HY conceived and designed the research. TT and HY performed the experiments, collected the data, prepared the figures, and conducted the simulation analysis. MY, SO, NH, and MN provided constructive suggestions and discussions. SO and HY reviewed and revised the manuscript. All authors were involved in the discussion of the results and writing of the manuscript.

**Funding** This research was partially supported by JSPS KAKENHI Grant Number 20K19362.

## Declarations

**Ethics approval** Experimental measurements using a cadaver were performed according to the protocol approved by the Ethics Committee of Aichi Medical University (Permit Number: 2019-M003).

**Conflicts of interest** The authors declared no potential conflicts of interest regarding the research, authorship, and/or publication of this article.

## References

- Akkaya N, Akkaya S, Gungor HR, Yaşar G, Atalay NS, Sahin F (2017) Effects of weighted and un-weighted pendulum exercises on ultrasonographic acromiohumeral distance in patients with subacromial impingement syndrome. *J Back Musculoskelet Rehabil* 30:221–228
- Aurbach M, Spicka J, Süß F, Dendorfer S (2020) Evaluation of musculoskeletal modelling parameters of the shoulder complex during humeral abduction above 90°. *J Biomech* 106:109817
- BodyParts3D/Anatomography (2008) Database Center for Life Science. <http://lifesciencedb.jp/bp3d/>.
- Buchanan TS, Lloyd DG, Manal K, Besier TF (2004) Neuromusculoskeletal modeling: estimation of muscle forces and joint moments and movements from measurements of neural command. *J Appl Biomech* 20:367–395
- Bullet BP (2015). Library. <http://bulletphysics.org> (Accessed 21/3/2022).
- Chadwick EK, Blana D, Kirsch RF, van den Bogert AJ (2014) Real-time simulation of three-dimensional shoulder girdle and arm dynamics. *IEEE Trans Bio Med Eng* 61:1947–1956
- Chopp JN, Dickerson CR (2012) Resolving the contributions of fatigue-induced migration and scapular reorientation on the subacromial space: an orthopaedic geometric simulation analysis. *Hum Mov Sci* 31:448–460
- Debski RE, Sakone M, Woo SL, Wong EK, Fu FH, Warner JJ (1999) Contribution of the passive properties of the rotator cuff to glenohumeral stability during anterior-posterior loading. *J Shoulder Elbow Surg* 8:324–329
- Enoka RM (2015) *Neuromechanics of human movement*, 5th edn. Human Kinetics.
- Flores-Hernandez C, Eskinazi I, Hoenecke HR, D'Lima DD (2019) Scapulothoracic rhythm affects glenohumeral joint force. *JSES Open Access* 3:77–82
- Garving C, Jakob S, Bauer I, Nadjar R, Brunner UH (2017) Impingement syndrome of the shoulder. *Dtsch Arztebl Int* 114:765–776
- Giphart JE, van der Meijden OAJ, Millett PJ (2012) The effects of arm elevation on the 3-dimensional acromiohumeral distance: a biplane fluoroscopy study with normative data. *J Shoulder Elbow Surg* 21:1593–1600
- Gordon AM, Huxley AF, Julian FJ (1966) The variation in isometric tension with sarcomere length in vertebrate muscle fibres. *J Physiol* 184:170–192
- Halder AM, Zhao KD, Odriscoll SW, Morrey BF, An KN (2001) Dynamic contributions to superior shoulder stability. *J Orthop Res* 19:206–212
- Harrison AK, Flatow EL (2011) Subacromial impingement syndrome. *J Am Acad Orthop Surg* 19:701–708
- Hill AV (1938) The heat of shortening and the dynamic constants of muscle. *Proc R Soc Lond A* 126:136–195
- Holzbaur KRS, Murray WM, Delp SL (2005) A model of the upper extremity for simulating musculoskeletal surgery and analyzing neuromuscular control. *Ann Biomed Eng* 33:829–840
- Islan M, Blaya F, Pedro PS, D'Amato R, Urquijo EL, Juanes JA (2018) Analysis and fem simulation methodology of dynamic behavior of human rotator cuff in repetitive routines: musician case study. *J Med Syst* 42:55
- Kibler WB, Ludewig PM, McClure PW, Michener LA, Bak K, Sciascia AD (2013) Clinical implications of scapular dyskinesis in shoulder injury: the 2013 consensus statement from the 'Scapular Summit'. *Br J Sports Med* 47:877–885
- Leschinger T, Birgel S, Hackl M, Staat M, Müller LP, Wegmann K (2019) A musculoskeletal shoulder simulation of moment arms and joint reaction forces after medialization of the supraspinatus footprint in rotator cuff repair. *Comput Methods Biomech Biomed Engin* 22:595–604
- Lugo R, Kung P, Ma CB (2008) Shoulder biomechanics. *Eur J Radiol* 68:16–24
- Mamou K, Lengyel E, Peters EAK (2016) Volumetric hierarchical approximate convex decomposition. *Game Engine Gems* 3:141–158
- Marchi J, Blana D, Chadwick EK (2014) Glenohumeral stability during a hand-positioning task in previously injured shoulders. *Med Biol Eng Comput* 52:251–256
- Masi AT, Hannon JC (2008) Human resting muscle tone (HRMT): narrative introduction and modern concepts. *J Bodyw Mov Ther* 12:320–332
- Massimini DF, Boyer PJ, Papannagari R, Gill TJ, Warner JP, Li G (2012) In-vivo glenohumeral translation and ligament elongation during abduction and abduction with internal and external rotation. *J Orthop Surg Res* 7:29
- McCully SP, Suprak DN, Kosek P, Karduna AR (2007) Suprascapular nerve block results in a compensatory increase in deltoid muscle activity. *J Biomech* 40:1839–1846
- Moskal MJ, Harryman DT, Romeo AA, Rhee YG, Sidles JA (1999) Glenohumeral motion after complete capsular release. *Arthroscopy* 15:408–416
- Müller M, Chentanez N, Kim TY (2013) Real time dynamic fracture with volumetric approximate convex decompositions. *ACM Trans Graph* 32:1–10

- Neumann DA, Garceau LR (2015) A proposed novel function of the psoas minor revealed through cadaver dissection. *Clin Anat* 28:243–252
- Neumann DA (2016) *Kinesiology of the musculoskeletal system—e-book: foundations for rehabilitation*. Elsevier Health Sciences, Amsterdam
- Paletta GA Jr, Warner JJP, Warren RF, Deutsch A, Altchek DW (1997) Shoulder kinematics with two-plane x-ray evaluation in patients with anterior instability or rotator cuff tearing. *J Shoulder Elbow Surg* 6:516–527
- Péan F, Tanner C, Gerber C, Fürnstahl P, Orcun G (2019) A comprehensive and volumetric musculoskeletal model for the dynamic simulation of the shoulder function. *Comput Methods Biomech Biomed Engin* 22:740–751
- Rafael FE, Kyle Y, Lonnie P, James RA (2009) Shoulder muscle activity and function in common shoulder rehabilitation exercises. *Sports Med* 39(8):663–685
- Sharkey NA, Marder RA (1995) The rotator cuff opposes superior translation of the humeral head. *Am J Sports Med* 23:270–275
- Styer-Acevedo J (1999) *Physical therapy for the child with cerebral palsy* *Pediatr Phys Ther*, 3rd edn. Lippincott Williams & Wilkins, Philadelphia
- Thelen DG (2003) Adjustment of muscle mechanics model parameters to simulate dynamic contractions in older adults. *J Biomech Eng* 125:70–77
- Veeger HEJ, van der Helm FCT (2007) Shoulder function: the perfect compromise between mobility and stability. *J Biomech* 40:2119–2129
- Vidt ME, Santago AC 2nd, Marsh AP et al (2018) Modeling a rotator cuff tear: individualized shoulder muscle forces influence glenohumeral joint contact force predictions. *Clin Biomech (bristol Avon)* 60:20–29
- Warner JJP, Deng XH, Warren RF, Torzilli PA (1992) Static capsulo-ligamentous restraints to superior-inferior translation of the glenohumeral joint. *Am J Sports Med* 20:675–685. <https://doi.org/10.1177/036354659202000608>
- Yang C, Goto A, Sahara W, Yoshikawa H, Sugamoto K (2010) In vivo three-dimensional evaluation of the functional length of glenohumeral ligaments. *Clin Biomech (bristol Avon)* 25:137–141
- Zajac FE (1989) Muscle and tendon: properties, models, scaling, and application to biomechanics and motor control. *Crit Rev Biomed Eng* 17:359–411
- Zheng M, Zou Z, Bartolo PJ, Peach C, Ren L (2017) Finite element models of the human shoulder complex: a review of their clinical implications and modelling techniques. *Int J Numer Method Biomed Eng* 33:e02777

**Publisher's Note** Springer Nature remains neutral with regard to jurisdictional claims in published maps and institutional affiliations.

Springer Nature or its licensor (e.g. a society or other partner) holds exclusive rights to this article under a publishing agreement with the author(s) or other rightsholder(s); author self-archiving of the accepted manuscript version of this article is solely governed by the terms of such publishing agreement and applicable law.